ARTICLES

High-pressure x-ray diffraction, absorption, luminescence, and Raman-scattering study of Cs_2MoS_4

B. Lorenz
Texas Center for Superconductivity, University of Houston, Houston, Texas 77204-5932

I. Orgzall
Hochdrucklabor bei der Universität Potsdam, Telegrafenberg A43, D-14473 Potsdam, Germany

P. K. Dorhout and C. C. Raymond
Department of Chemistry, Colorado State University, Fort Collins, Colorado 80523

K. Brister
CHESS, Wilson Laboratory, Cornell University, Ithaca, New York 14853

K. Weishaupt, R. D'Adamo, and H. D. Hochheimer
Department of Physics, Colorado State University, Fort Collins, Colorado 80523
(Received 12 February 1996; revised manuscript received 5 August 1996)

Cesium thiomolybdate, Cs_2MoS_4, has been investigated at pressures up to 12 GPa. Two phase transitions have been detected by absorption measurements, Raman spectroscopy, and energy dispersive x-ray diffraction. The first phase transition to a monoclinic phase II [$a=14.061(9)$ Å, $b=11.552(7)$ Å, $c=9.852(6)$ Å, $\beta=97.14(6)°$] has been observed at 8.0 GPa. The second transition at 9.7 GPa has been observed from the monoclinic phase II to an orthorhombic phase III [$a=12.085(4)$ Å, $b=15.707(6)$ Å, $c=11.828(5)$ Å]. Absorption and luminescence measurements have indicated an increase in the absorption edge energy with pressure up to ~3 GPa. At pressures greater than 3.5 GPa, the absorption energy decreases. Raman spectroscopy has revealed a low-frequency phonon mode with a negative pressure shift in the low-pressure phase I. The pressure-temperature phase diagram has been determined up to 250 °C. The transition pressures decrease linearly with slopes of ~ -0.013 GPa/°C. Models for the pressure-induced structural and electronic transitions are proposed. [S0163-1829(97)06305-4]

I. INTRODUCTION

Recent studies of divalent molybdates[1–3] have revealed the existence of pressure-induced phase transitions in these materials. Jayaraman *et al.* have even reported pressure induced amorphization in Tb and Gd trimolybdates at a moderate pressure of 6 GPa.[4,5] Furthermore, they have found a spectacular pressure induced electronic transition in $KTb(MoO_4)_2$, which they attribute to $4f$-$5d$ transition in Tb initiated by the structural transition and consequent intervalence charge transfer between Tb and Mo.[6] These results in combination with the fact that molybdenum sulfides are important in bioorganic chemistry and heterogeneous catalysis[7,8] generated the interest to study molybdenum sulfides. The fact that samples of Cs_2MoS_4 have been successfully synthesized, as well as no high-pressure studies have been performed on this material before to the best of our knowledge, motivated us to study the physical properties of Cs_2MoS_4 at ambient and high pressures using energy-dispersive x-ray diffraction, absorption, and luminescence measurements, and Raman spectroscopy. The optical studies indicated the existence of two high-pressure phase transitions at 8 and 9.7 GPa. These phase transitions have been confirmed with energy-dispersive x-ray diffraction and the structure was determined to be monoclinic with a space group based on descend in symmetry of $P2_1/c$ for phase II above 8 GPa and to be orthorhombic for phase III above 9.7 GPa. The structural data provided the base for an interpretation of the interesting results of the absorption, luminescence, and Raman scattering measurements, which will be presented in this paper.

II. EXPERIMENT

Single crystals of Cs_2MoS_4 were prepared as reported earlier[9] by the hydrothermal reaction of molybdenum powder with K_2S_6 and K_2Se_4 (a sacrifical oxidant) in 500 μl of a 1.0-M cesium acetate solution. The compound crystallizes as orange needles.

High-pressure measurements were performed using the gasketed diamond-anvil-cell technique. The Inconel gasket was preindented to a thickness of 0.1 mm and a hole of 0.2-mm diameter forms the sample chamber. The energy-dispersive x-ray measurements were performed at the beam-

 © 1997 The American Physical Society

line $B1$ at the Cornell High Energy Synchrotron Source (CHESS)[10] using powdered material mixed with NaCl for pressure determination. The broad reflections of the NaCl pressure sensor, which in same cases even overlapped with reflections of the sample, resulted in a rather large error (± 0.2 to 1.0 GPa). For the optical measurements a single crystal with a typical size of 0.05 mm was loaded into the gasket hole together with a small chip of Sm^{2+} doped SrFCl used as a pressure sensor. This luminescence sensor was used instead of the standard ruby sensor in order to increase the precision of the pressure measurements.[11] A 4:1 mixture of methanol and ethanol was used as the pressure transmitting medium for the Raman and absorption measurements up to 12 GPa. This guaranteed hydrostatic conditions up to at least 10 GPa. For the low-pressure ($P<3$ GPa) luminescence measurements paraffin oil was used to ensure hydrostatic conditions.

The sample was excited by a He-Ne laser (632.8 nm) for the Raman measurements. In order to avoid thermal heating the laser power was reduced to less than 4 mW. The Raman spectra were recorded using a triple spectrograph ''T64000'' (Instruments SA) with a liquid nitrogen cooled CCD detector. The resolution was less than 1 cm^{-1}. For the luminescence measurements the sample was excited with the 488-nm line of an argon laser and the luminescence intensity was recorded with a $\frac{1}{4}$-m Czerny-Turner spectrograph ''SP 275'' (Acton Research Corp.) and a Peltier-cooled CCD detector. The incident laser beam was focused on the sample with a typical spot size of 8 μm for these measurements. For the optical absorption studies, a quartz-tungsten-halogen light source and the same detection system as for the luminescence measurements was used. The reference spectrum was measured beside the sample through the diamond-anvil cell. This reduced possible errors due to the absorption by the diamonds and the pressure medium.

The measurements above room temperature for the determination of the phase diagram were made using a high-pressure cell with an internal ring heater. The heater consisted of a Thermocoax heating wire (Philips) embedded in a high-temperature ceramic adhesive. Its construction was similar to the heater described by Li and Jeanloz.[12] The temperature was measured using a K-type thermocouple in contact with the diamond anvil. This temperature was related to the sample temperature in the gasket hole by a calibration function. The calibration curve was measured at ambient pressure with a thermocouple at the outside of the anvil and one inside the sample chamber in analogy to the procedure outlined in Ref. 20. The temperature inside the cell was roughly $\frac{3}{4}$ of the temperature measured at the diamond anvil. The estimated error in temperature measurement was about 5 K.

III. RESULTS AND DISCUSSION

A. Energy-dispersive x-ray measurements

Cs_2MoS_4 is a member of the class of A_2BX_4 compounds which are isostructural with β-K_2SO_4.[13] The structure of the low-pressure phase I is built up from $[MoS_4]^{2-}$ clusters and Cs^+ ions forming an orthorhombic lattice with four formula units in the Bravais cell (Fig. 1) (space group D_{2h}^{16} or $Pnma$).[9] Figure 2 shows the energy-dispersive powder x-ray

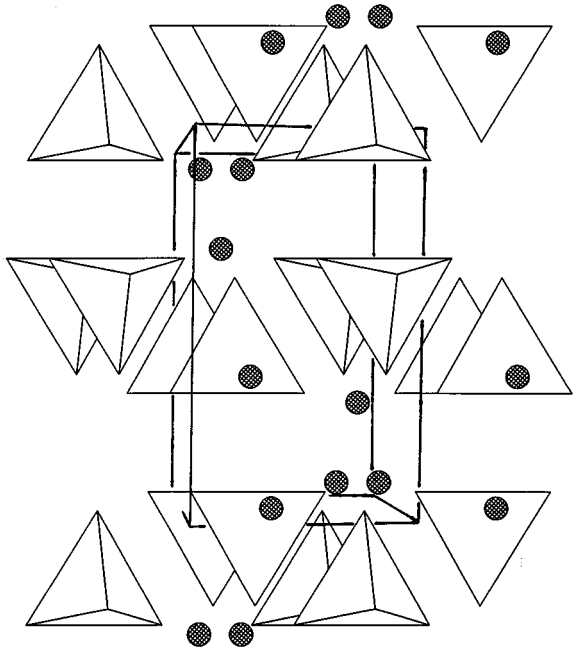

FIG. 1. Bravais cell of Cs_2MoS_4. View is along the x axis of the orthorhombic cell.

diffraction patterns of Cs_2MoS_4 in low-pressure phase I and in the two high-pressure phases II and III, respectively. The peak positions were determined by fitting each peak or overlapping peaks with a Gaussian function. The energy of the peak was converted using Bragg's Law and the angle of the detector, which was determined using a gold foil. The indexing of the reflections was performed with Proszki[14] and the unit-cell refinements were performed with U fit.[15]

The hkl values are listed in Tables I and II together with the observed and calculated d values of the reflections observed in phase II and III, respectively. Problems such as preferential orientation and variations in incident x-ray flux prevented the evaluation of intensity data for the structure determination. It can be seen that the indexing agrees well with the structural parameters listed in Table III. The number of formula units in the unit cells of phase II and III are based on densities determined from a fit of the Birch equation of state to the measured pressure-volume data points.

Though high-pressure powder x-ray diffraction data do not normally allow the determination of the space group, we suggest that the space group of phase II is $P2_1/c$ based on descent in symmetry. Kawada *et al.*[16] have found a monoclinic high-pressure form of $BaWO_4$ with space group $P2_1/n$, which is a nonstandard setting of the space group $P2_1/c$. They pointed out that the high-pressure structure contains densely packed two-dimensional networks of WO_6 octahedra. Monoclinic high-pressure phases have also been found in $SrMoO_4$,[1] $CaMoO_4$,[2] and $CdMoO_4$.[3] Since the phase transitions to monoclinic high-pressure phases of these materials were accompanied by a coordination number change from 4 to 6, the transition to phase II in the case of Cs_2MoS_4 may be explained as in the case of $BaWO_4$ (Ref. 16) (Fig. 3).

The y axis of the orthorhombic low-pressure phase I is doubled and becomes the x' axis in the monoclinic high-pressure phase II. The x and z axis of phase I become the z'

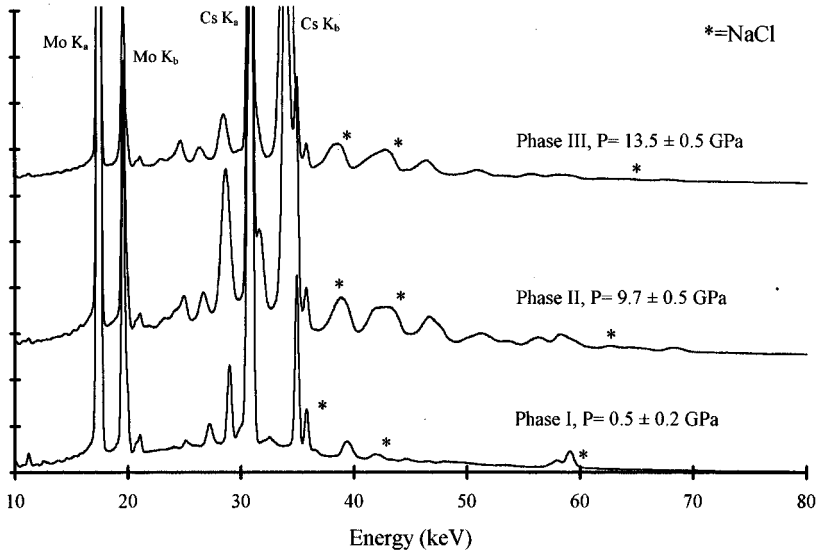

FIG. 2. Powder x-ray diffraction patterns of Cs_2MoS_4 in phase I, II, and III.

and y' axis of phase II. The denser packing in the high-pressure phase leads to a change in the coordination number from 4 to 6 and creates a layered structure in the y'-z' plane [Fig. 3(c)]. This picture is strongly supported by the results of the Raman study, which will be presented next.

B. Raman measurements

The Raman spectrum of the low-pressure phase I is characterized by well separated internal modes of the strongly bonded $[MoS_4]^{2-}$ molecule and the external lattice vibrations below 100 cm^{-1}.[17] The internal modes resulting from the fundamental vibrations of the $[MoS_4]^{2-}$ tetrahedron have been investigated using IR and Raman spectroscopy.[18] According to the T_d symmetry of the $[MoS_4]^{2-}$ ion, group theory predicts four modes with symmetry A_1, E, and 2 F_2. Since two of these modes (E and F_2) are accidentally degenerate, three lines are observed at 458 cm^{-1} (A_1), 472 cm^{-1} (F_2), and 184 cm^{-1} ($E+F_2$) in the Raman spectra of the ion in aqueous solution.[18] In the crystalline structure of the salt,[9] the degeneracies are lifted and the internal modes appear as vibrational bands in the vicinity of these energies. Müller *et al.*[19,20] have shown that the F_2 and the $(E+F_2)$ modes

TABLE I. hkl-values and observed and calculated d values in the high-pressure phase II at 7.8±0.5 GPa.

hkl	$d_{(obs)}$	$d_{(calc)}$
00$\bar{2}$	4.906	4.888
121	4.759	4.781
220	4.455	4.449
112	4.141	4.148
311	3.790	3.789
022	3.732	3.731
40$\bar{0}$	3.489	3.488
312	3.447	3.437
30$\bar{2}$	3.174	3.178
20$\bar{3}$	3.108	3.104
132	3.005	3.004
13$\bar{2}$	2.908	2.910
232	2.852	2.856
500	2.791	2.790
213	2.742	2.741
51$\bar{0}$	2.711	2.712
40$\bar{3}$	2.543	2.544
41$\bar{3}$	2.482	2.485
43$\bar{2}$	2.375	2.377
601	2.330	2.328
05$\bar{0}$	2.311	2.310
333	2.289	2.285
25$\bar{1}$	2.121	2.122
41$\bar{4}$	2.094	2.094
25$\bar{2}$	2.034	2.030
424	1.996	1.998

TABLE II. hkl values and observed and calculated d values in the high-pressure phase III at 12.5±0.5 GPa.

hkl	$d_{(obs)}$	$d_{(calc)}$
211	5.097	5.091
220	4.784	4.789
031	4.784	4.788
022	4.730	4.724
131	4.448	4.451
103	3.745	3.748
321	3.432	3.430
322	3.069	3.065
400	3.025	3.021
114	2.826	2.825
043	2.784	2.782
421	2.740	2.743
124	2.698	2.698
342	2.536	2.539
333	2.481	2.481
413	2.372	2.371
520	2.310	2.310
170	2.208	2.206
270	2.103	2.103
344	2.036	2.038
165	1.737	1.737
710	1.716	1.716

TABLE III. Unit-cell parameters for phases I, II, and III.

	Phase I (Ref. 17) (ambient pressure)	Phase II (7.8±0.5 GPa)	Phase III (12.5±0.5 GPa)
a, Å	10.0479(7)	14.061(9)	12.085(4)
b, Å	7.2463(4)	11.552(7)	15.707(6)
c, Å	12.783(1)	9.852(7)	11.828(5)
α	90	90	90
β	90	97.14(6)	90
γ	90	90	90
Formula Units	4	8	12
R[a]		0.044	0.026

[a]The R value is defined as:

$$R=\frac{\Sigma(2\theta_{(\mathrm{obs})}-2\theta_{(\mathrm{calc})})^2}{(N_{(\mathrm{hkl})}-N_{(\mathrm{var})})},$$

where $N_{(\mathrm{hkl})}$ and $N_{(\mathrm{var})}$ are the number of data points and variables, respectively.

split into two Raman lines. Recent Raman measurements show up to five different lines for the F_2 modes near 470 cm^{-1} and four lines in the band around 180 cm^{-1} $(E+F_2)$.[17] The external modes of Cs_2MoS_4 were observed in those experiments.

The vibrational spectrum of phase I of the Cs_2MoS_4 crystal can be analyzed using the standard factor group analysis. The Cs and Mo ions have site symmetry C_s. Factor group analysis using the correlation $\sigma(z,x)$ for C_s in D_{2h} yields that 42 Raman modes are allowed by symmetry. 18 external modes with symmetry $6A_g+6B_{2g}+3B_{1g}+3B_{3g}$, 6 librational modes with symmetry $A_g+B_{2g}+2B_{1g}+2B_{3g}$, and again 18 internal modes with symmetry $6A_g+6B_{2g}+3B_{1g}+3B_{3g}$. The last result was obtained by applying the same correlation to the four modes with symmetry A, E, and 2 F_2 of the $[MoS_4]^{2-}$ tetrahedral ion with T_d symmetry.

The room-temperature Raman spectra of the three phases are shown in Fig. 4. At ambient pressure the external modes

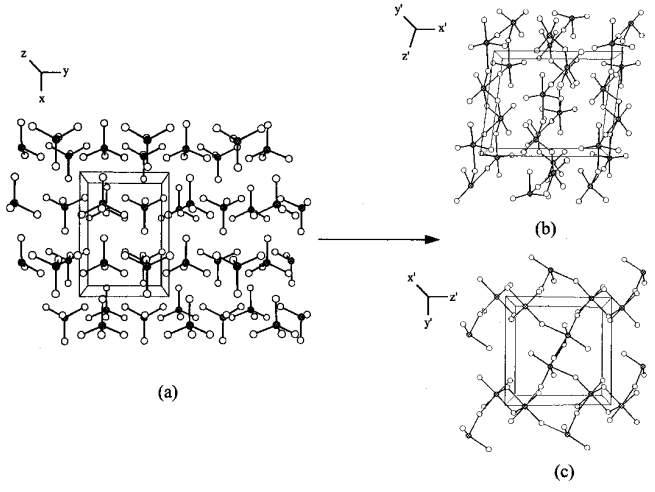

FIG. 3. (a) Top view on the x-y plane in the low-pressure orthorhombic phase I; (b) Top view on the x'-z' plane in the monoclinic high-pressure phase II; (c) Layered structure in the y'-z' plane of the monoclinic high-pressure phase II. Cs-ions are not shown for clarity in (a), (b), and (c).

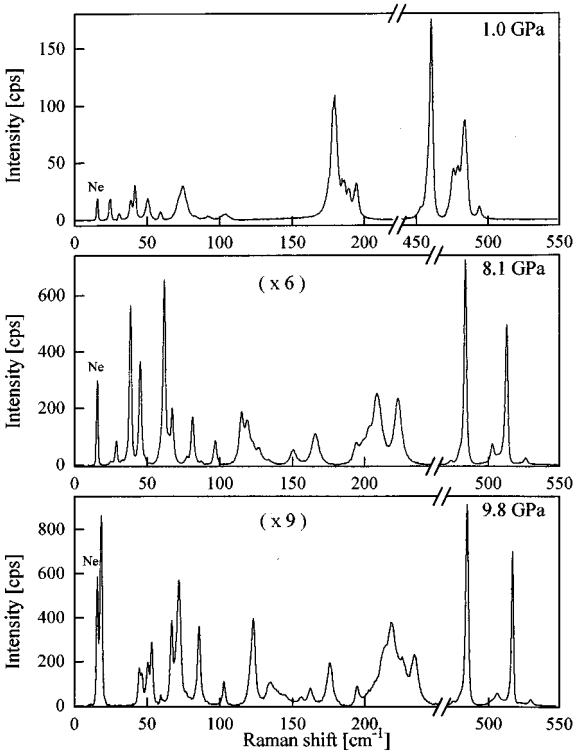

FIG. 4. Room-temperature Raman spectra at different pressures.

below 100 cm^{-1} are clearly separated from the internal ones above 170 cm^{-1} by a gap of 80 cm^{-1}. Due to the stronger pressure shift of the external modes this gap becomes smaller. However, at the highest pressures in this experiment (12 GPa) the internal modes are still separated by about 15 cm^{-1} from the external ones.

The pressure shifts of all Raman active modes are shown in Figs. 5(a), 5(b), and 5(c). The values of the mode frequencies at ambient pressure and of the pressure derivatives, $d\ \ln\ \nu/dP$, at room temperature are compiled in Table IV and plotted in Fig. 6. It is interesting to note that the four lowest frequency external modes ($\nu_1-\nu_4$ below 40 cm^{-1}) have anomalous small pressure derivatives, and even more important that the mode ν_2 has a negative pressure coefficient [Table IV and Fig. 5(a)]. With increasing pressure ν_2 crosses the lowest mode ν_1 and becomes the lowest frequency phonon above 4.5 GPa. At the first phase transformation this phonon vanishes completely suggesting that the change of structure is related to the phonon softening.

A softening of a low-frequency mode involving $MoO_4^{2-}-MoO_4^{2-}$ stretching in the low-pressure phase as well as a downward shift of stretching vibrations within the M-O polyhedron (M=W, Mo) in the high-pressure phase was also observed in $CaMoO_4$,[2] $SrMoO_4$,[1] and $BaWO_4$.[21] Jayaraman *et al.*[1,21] and Christofilos *et al.*[2] pointed out that this behavior is connected with an increase of the coordination number of the metal ion in the high-pressure phase. We also observe such a behavior in Cs_2MoS_4. Therefore, the results of our Raman study support the proposed model based on x-ray diffraction for phase II, presented in Sec. III A.

C. Phase diagram

In order to determine the phase diagram of Cs_2MoS_4, high-pressure–high-temperature measurements were per-

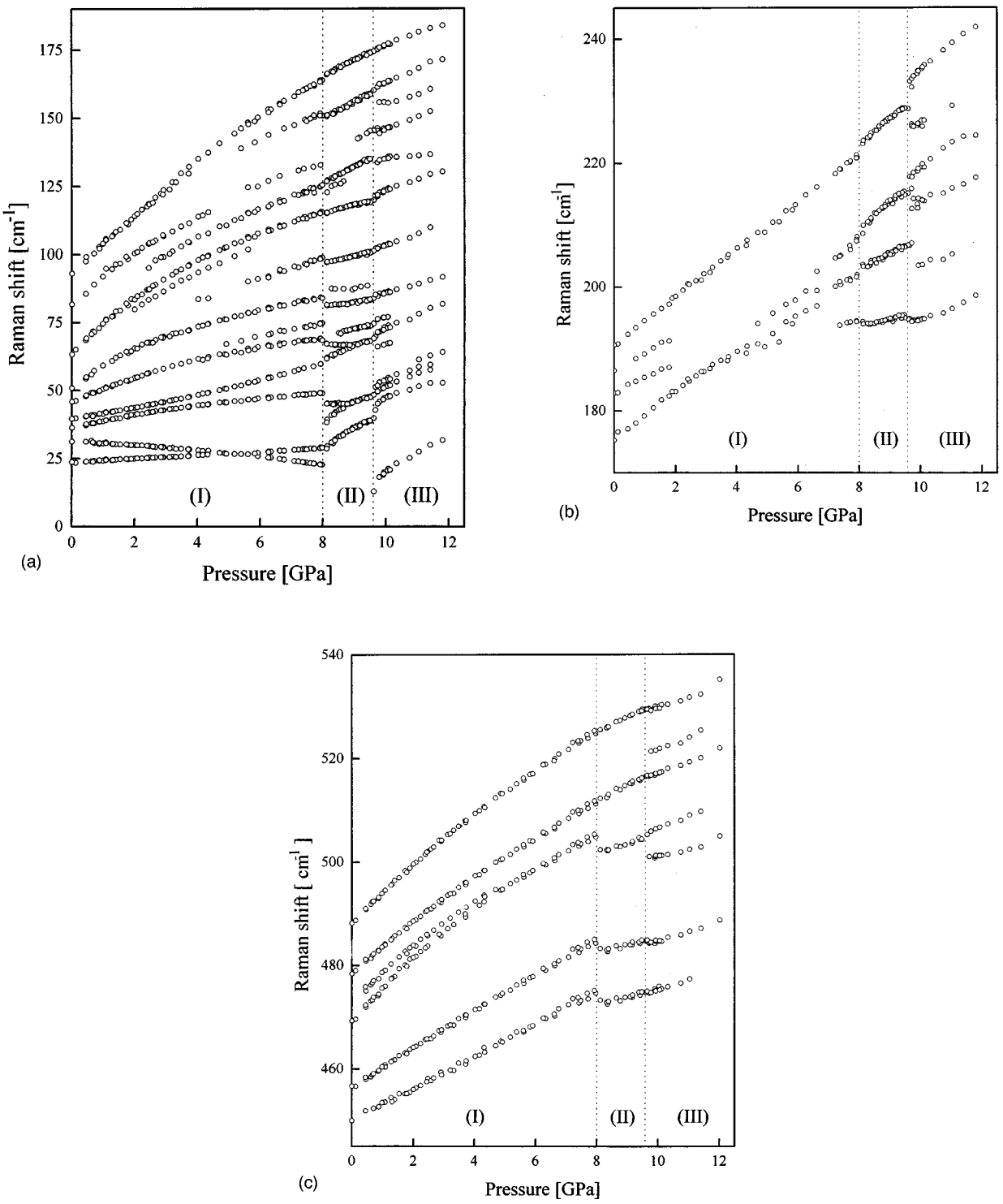

FIG. 5. Pressure dependence of the Raman active modes of Cs_2MoS_4. (a) external modes; (b) internal modes around 180 cm^{-1}; (c) internal modes above 450 cm^{-1}. The low-pressure phase is labeled with (I), and the two high-pressure phases with (II) and (III), respectively.

formed. The abrupt changes of the Raman spectra (external modes) have been used to estimate the transition pressures of both phase transformations. Figure 7 shows the phase diagram from room temperature to 250 °C and for pressures up to 10 GPa. The high-pressure phases (II) and (III) extend to lower pressures with increasing temperature. The phase boundaries are well defined and slightly curved with an average slope of -0.013 GPa/°C, and cycling several times through the transitions showed no hysteresis. The width of the transitions is smaller than the error in pressure determination indicated by the error bars in Fig. 7.

The absence of a hysteresis in the transition to phase II as well as the presence of a soft phonon mode suggest a second order phase transition driven by a soft mode. On the other hand, a first-order transition with a very small transition enthalpy cannot be ruled out, especially as the almost linear pressure dependence of the soft mode provides evidence for the nonexistence of any critical exponent. Such scaling be-

TABLE IV. Mode frequencies and pressure derivatives of the Raman active modes in the low-pressure phase of Cs_2MoS_4.

Mode	Frequency ($p=0$) (cm^{-1})	Pressure derivative $d \ln \nu/dp$ (GPa^{-1})
ν_1	23.8	0.022
ν_2	31.2	−0.016
ν_3	36.3	0.07
ν_4	39.7	0.046
ν_5	45.9	0.107
ν_6	50.9	0.18
ν_7	63.3	0.144
ν_8	64.9	0.156
ν_9	76.3	0.115
ν_{10}	81.7	0.131
ν_{11}	93.1	0.112
ν_{12}	175.2	0.025
ν_{13}	182.8	0.014
ν_{14}	186.5	0.015
ν_{15}	190.6	0.021
ν_{16}	450	0.007
ν_{17}	456.7	0.008
ν_{18}	469.3	0.015
ν_{19}	473.9	0.011
ν_{20}	478.4	0.011
ν_{21}	488.3	0.012

havior, however, is crucial for a second-order transition. Furthermore, we were able to record Raman spectra showing the characteristic features of two coexisting phases. If we exclude pressure gradients this again indicates that the transitions are of first order.

D. Absorption and luminescence measurements

Selected absorption spectra at different pressures are shown in Fig. 8; the absorption edge was determined from the intersection of the two straight lines A and B. The pressure dependence of the absorption edge is displayed in Fig. 9. Two phase transitions are clearly reflected in abrupt changes of the edge energy, E, at the transition pressures of 8.0 and 9.7 GPa in agreement with the transitions observed in the Raman data. At the first transition, E suddenly decreases by about 50 meV and then continues to decrease linearly with pressure in phase II. At 9.7 GPa, the edge energy jumps back to its value at 8 GPa (phase II) followed by a decrease in E upon increasing pressure in phase III.

The most interesting feature of the pressure dependence of the edge energy in the low-pressure phase I is the sign change of the pressure derivative, dE/dP, at about 3.5 GPa. The pressure dependence of the absorption edge in the low-pressure phase can be described by a quadratic equation

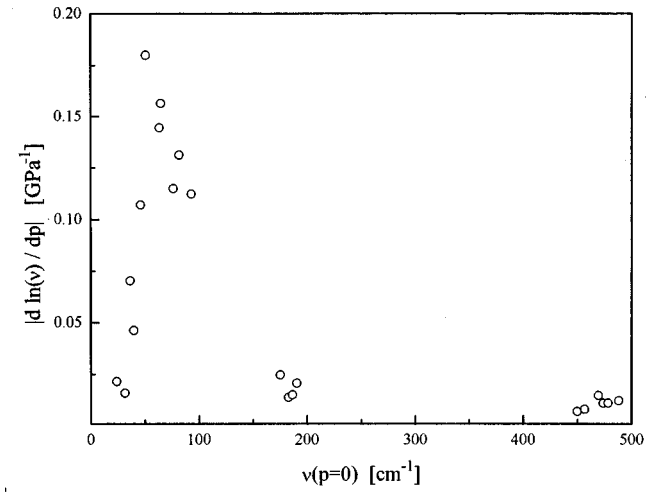

FIG. 6. Absolute values of the pressure derivatives, $d \ln \nu/dp$, of the mode frequencies versus $\nu(p=0)$.

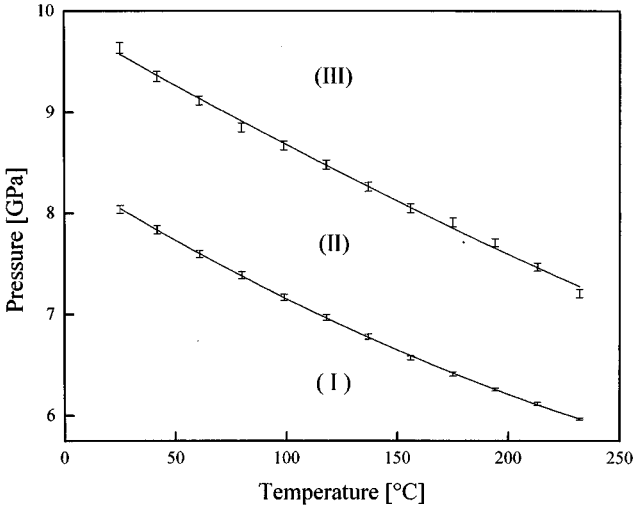

FIG. 7. Phase diagram of Cs_2MoS_4.

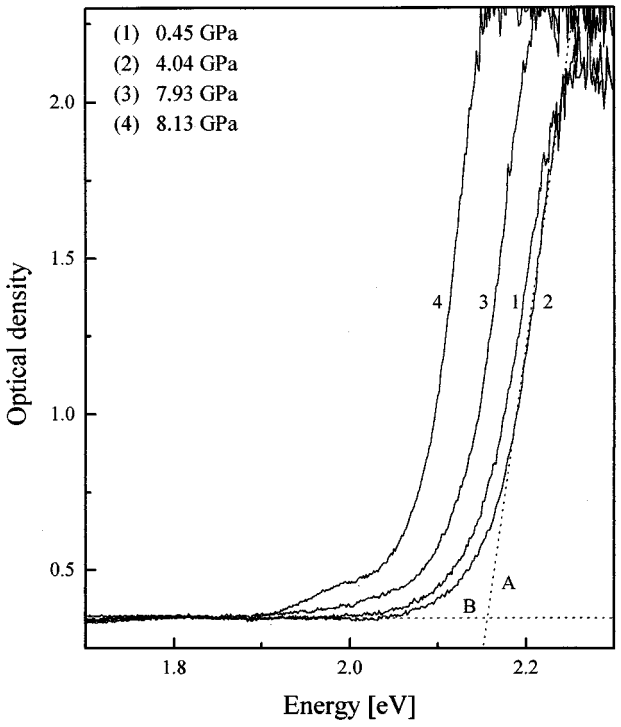

FIG. 8. Room-temperature absorption spectra at different pressures. The absorption edge is defined by the intersection of the straight lines A and B.

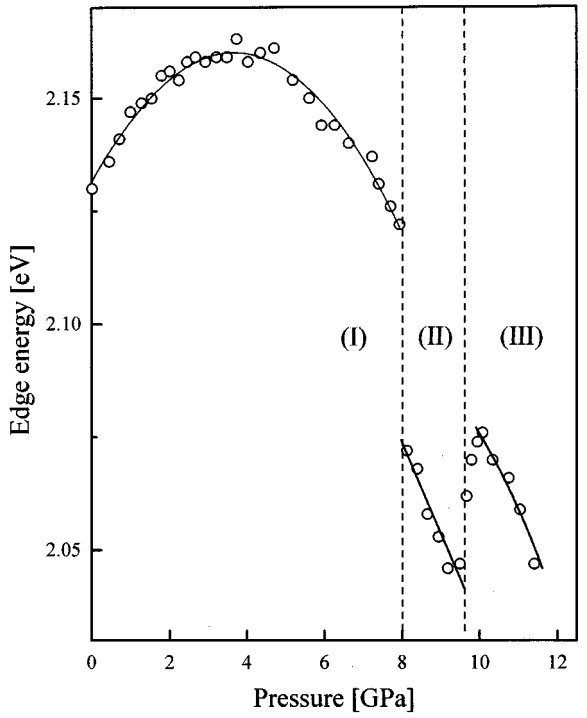

FIG. 9. Pressure dependence of the absorption edge.

$$E(\mathrm{eV}) = a_0 + a_1 P + a_2 P^2 \quad (P \text{ in GPa})$$

with $a_0 = 2.132(1)$ eV, $a_1 = 0.0155(7)$ eV/GPa, and $a_2 = -0.0021(1)$ eV/GPa^2. This behavior implies that the electronic structure is more complicated than that of a typical semiconductor; there is no well-defined single gap in the band structure which determines the optical properties. The change of sign of dE/dP indicates that a band crossing may occur with increasing pressure.

In order to provide further support for a direct-indirect band crossing, luminescence measurements were performed. High-pressure investigations of GaAs[22–24] and InP[25–27] have shown that a direct-indirect band crossing results in a characteristic decrease of the luminescence intensity across the direct gap. Selected luminescence spectra at different pressures are shown in Fig. 10. The spectra are corrected by subtracting the Raman and resonance Raman lines of the sample as well as the luminescence signal of the diamond anvils and of the pressure medium. The maximum of the luminescence intensity shifts to higher energies up to 3 GPa, with a concomitant decrease of the integrated intensity by about one order of magnitude (Fig. 11). Due to the necessary corrections of the spectra, the relative error of the integrated intensities is about 10%. However, the intensity decrease with pressure is well established by the plot in Fig. 11.

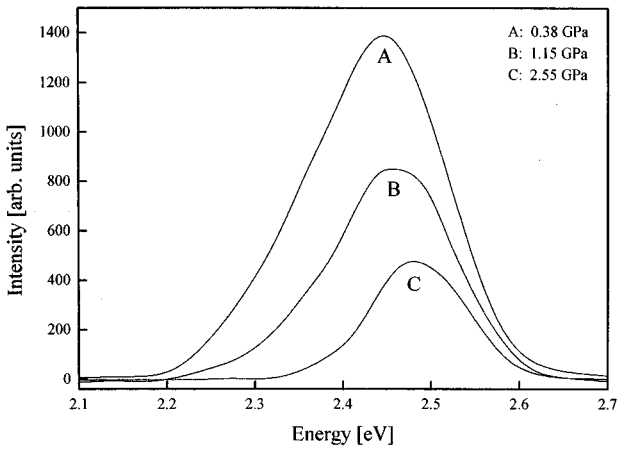

FIG. 10. Room-temperature luminescence spectra at different pressures.

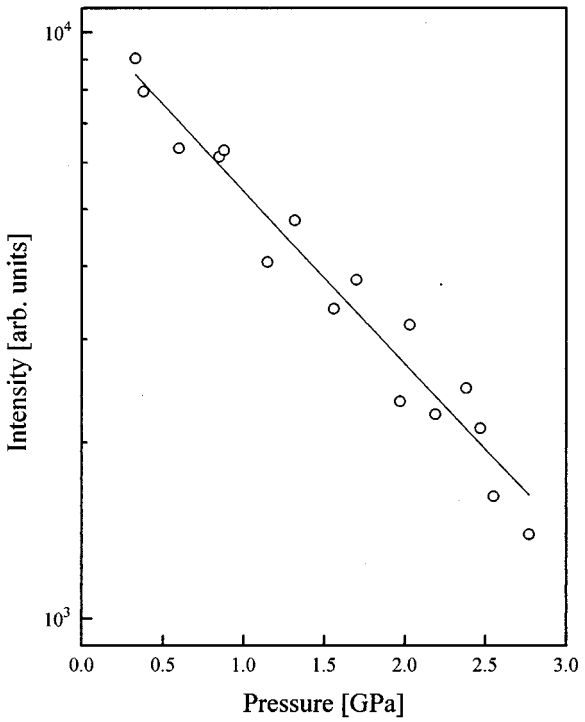

FIG. 11. Integrated luminescence intensities versus pressure.

The luminescence maximum shifts to higher energy, which is related to the opening of the direct gap at the Γ point of the Brillouin zone with increasing pressure. This shift is about 30 meV from ambient pressure to 3 GPa and is comparable with the shift of the absorption edge in the same pressure range (Fig. 9). However, at ambient pressure the position of the maximum (2.46 eV) is 300-meV higher than the absorption edge, indicating that excitonic states below the conduction band are probably responsible for the observed absorption.

Based on the results of the absorption and luminescence measurements we propose a qualitative scheme (Fig. 12) to explain the effect of pressure on the electronic excitation spectrum. At ambient pressure the onset of absorption is determined by excitations into excitonic levels, which are about 0.3 eV below the conduction band at the Γ point of the Brillouin zone. The photoluminescence is due to the recombination of charge carriers from the bottom of the conduction band (2.46 eV above the valence band) at the Γ point. The fact that the luminescence intensity (Fig. 11) shows no plateau, as in the case of InP,[25–27] indicates that there is at least one more local minimum in the conduction band at another point in the Brillouin zone, most probably at a zone boundary. This minimum forms an indirect gap with the valence band. The width of this indirect gap is expected to be of similar size as the direct one, so that a portion of the photoexcited carriers does not take part in the luminescence process [Fig. 12(a)].

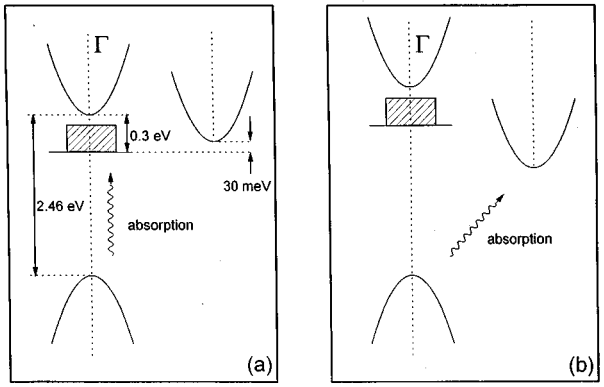

FIG. 12. Schematic band structure diagram compiling the results of the absorption and luminescence measurements.

The fact that we do not see the plateau in the luminescence intensity prevents a fit of our data to a theoretical formula for the luminescence intensity derived by Kobayashi *et al.*[26] One of the parameters of the expression for the pressure dependence of the emission intensity is the transition pressure of the direct indirect band crossing. Jayaraman *et al.*[1] report a decrease in the optical gap with increasing pressure in $SrMoO_4$. They claim that it appears also from their observations on other molybdates[21,28] that the *d* state of the Mo ion decreases in energy with increasing pressure, thus reducing the optical energy gap of the material. However, they do not refer to an indirect gap. Based on the results of our luminescence measurements, we favor the direct indirect band crossing picture.

Only detailed band structure calculations will provide an unambiguous answer which picture will be right. We hope that the results presented here together with results of Jayaraman *et al.*[1,21,28] will motivate such calculations.

IV. SUMMARY

We have observed two high-pressure phase transitions with no measurable hysteresis and a very small transition region in Cs_2MoS_4. The structure of the high-pressure phases was determined to be monoclinic and orthorhombic, respectively using energy-dispersive x-ray diffraction. The results from our Raman scattering study support that the coordination number increases at the transition to the first high-pressure phase. The observed decrease of a low-frequency external mode is explained with this increase of the coordination number. The electronic excitation spectrum is investigated by absorption and luminescence measurements. We have shown that the results can be explained by a band crossing model where above 3.5 GPa the optical absorption is determined by electronic excitations across an indirect gap. Band structure calculations are necessary to prove the occurrence of a direct-indirect band crossing.

ACKNOWLEDGMENTS

This work is partly based upon research conducted at the Cornell High Energy Synchrotron Source, which is supported by the National Science Foundation under Award No. DMR-93-11772. Furthermore, we acknowledge the support of the National Science Foundation through Grant Nos. DMR-93-10222 and CHE-96-25378.

[1] A. Jayaraman, S. Y. Wang, S. R. Shieh, S. K. Sharma, and L. C. Ming, J. Raman Spectrosc. **26**, 451 (1995).
[2] D. Christofilos, G. A. Kourouklis, and S. Ves, J. Phys. Chem. Solids **56**, 1125 (1995).
[3] A. Jayaraman, S. Y. Wang, and S. K. Sharma, Phys. Rev. B **52**, 9886 (1995).
[4] A. Jayaraman, S. K. Sharma, Z. Wang, S. Y. Wang, L. C. Ming, and M. H. Manghnani, J. Phys. Chem. Solids **54**, 827 (1993).
[5] A. Jayaraman, S. K. Sharma, and S. Y. Wang, Pramana **40**, 357 (1993).
[6] A. Jayaraman, S. Y. Wang, S. K. Sharma, and S.-W. Cheong, Curr. Sci. **7**, 232 (1996).
[7] D. Coucouvanis, Acc. Chem. Res. **14**, 201 (1981).
[8] R. R. Chianelli, Catal. Rev.-Sci. Eng. **26**, 361 (1984).
[9] C. C. Raymond, P. K. Dorhout, and S. M. Miller, Z. Kristallogr. **210**, 775 (1995).
[10] K. Brister, Nucl. Instrum. Methods A **319**, 333 (1992).
[11] B. Lorenz, Y. S. Shen, and W. B. Holzapfel, High Press. Res. **12**, 91 (1994).
[12] X. Li and R. Jeanloz, Phys. Rev. B **36**, 474 (1987).
[13] M. T. Robinson, J. Phys. Chem. **62**, 925 (1958).
[14] N. Lasocha, K. Lewinski, PROSZKI: A System of Programs for Powder Diffraction Data Analysis, Version 2.4 (Jagiellinian University, Poland, 1985).
[15] M. Evain, U-FIT: A Cell Parameter Refinement Program (I.M.N. Nantes, France, 1992).
[16] I. Kawada, K. Kato, and T. Fujita, Acta Crystallogr. B **30**, 2069 (1974).
[17] B. Lorenz, I. Orgzall, P. K. Dorhout, C. C. Raymond, and H. D. Hochheimer, Solid State Commun. **97**, 535 (1996).
[18] K. H. Schmidt and A. Müller, Coord. Chem. Rev. **14**, 115 (1974).
[19] A. Müller, N. Weinstock, and H. Schulze, Spectrochim. Acta **28A**, 1075 (1972).
[20] A. Müller, W. Jaegermann, and W. Hellmann, J. Mol. Struct. **100**, 559 (1983).
[21] A. Jayaraman, B. Batlogg, and L. G. VanUitert, Phys. Rev. B **28**, 4774 (1983).
[22] B. Welber, M. Cardona, C. K. Kim, and S. Rodriguez, Phys. Rev. B **12**, 5729 (1975).
[23] P. Y. Yu and B. Welber, Solid State Commun. **25**, 209 (1978).
[24] D. Olego, M. Cardona, and H. Müller, Phys. Rev. B **22**, 894 (1980).
[25] H. Müller, R. Trommer, M. Cardona, and P. Vogl, Phys. Rev. B **21**, 4879 (1980).
[26] T. Kobayashi, T. Tei, K. Aoki, K. Yamamoto, and K. Abe, in *Physics of Solids Under High Pressure*, edited by J. S. Schilling and R. N. Shelton (North-Holland, Amsterdam, 1981), p. 141.
[27] C. S. Menoni, H. D. Hochheimer, and I. L. Spain, Phys. Rev. B **33**, 5896 (1986).
[28] A. Jayaraman, S. Y. Wang, and S. K. Sharma, Solid State Commun. **93**, 885 (1995).